

# Mullite-rich plasma electrolytic oxide coatings for thermal barrier applications

J.A. Curran<sup>a</sup>, H. Kalkanç<sup>b</sup>, Yu. Magurova<sup>c</sup>, T.W. Clyne<sup>a,\*</sup>

<sup>a</sup> Department of Materials Science and Metallurgy, Cambridge University, Pembroke Street, Cambridge CB2 3QZ, UK

<sup>b</sup> Department of Metallurgical and Materials Engineering, Sakarya University, 54187 Sakarya, Turkey

<sup>c</sup> Moscow Institute of Steel and Alloys, 119235, Leninsky Prospekt 4, Moscow, Russia

Available online 1 September 2006

## Abstract

A study has been undertaken of the characteristics exhibited by mullite-rich plasma electrolytic oxide coatings grown on aluminium alloys by using silicate-rich electrolytes. It is found that they can be grown at a higher rate, and to a greater thickness, than alumina PEO coatings on aluminium. The thermal conductivity of these coatings has been measured using a steady-state method. It is shown to be of the order of  $0.5 \text{ W m}^{-1} \text{ K}^{-1}$ , which may be compared with  $\sim 1.5 \text{ W m}^{-1} \text{ K}^{-1}$  for pure alumina PEO coatings and  $\sim 10\text{--}15 \text{ W m}^{-1} \text{ K}^{-1}$  for dense polycrystalline mullite. Coupled with excellent substrate adhesion and good mechanical properties, this relatively low conductivity makes these coatings attractive for thermal barrier applications. Furthermore, they are shown to exhibit a relatively low global stiffness ( $\sim 40 \text{ GPa}$ ), which will reduce the magnitude of thermally-induced stresses and improve the resistance to spallation during temperature changes.

© 2006 Published by Elsevier B.V.

*Keywords:* PEO coatings; Mullite; Thermal conductivity; Thermal barrier; Alumina

## 1. Introduction

Plasma electrolytic oxide (PEO) coatings [1–4], which are sometimes referred to as micro-arc oxide coatings or spark/discharge anodic coatings, are formed by the oxidation of metal substrates in an aqueous electrolyte, via a series of localized electrical discharge events. These discharges allow oxide growth to proceed so as to produce films with thicknesses of the order of  $100 \mu\text{m}$  on aluminium. They have been explored and developed for various applications, particularly those in which wear resistance [5–10] and corrosion resistance [7,9,11] are required. Among the attractions of the process are that it involves very few health or safety hazards, and that coatings of uniform thickness can quickly and easily be produced on components with complex surface geometry, over a wide range of sizes. Because substrate conversion is involved, rather than simple deposition, the interfacial adhesion is usually excellent.

Thermal protection [12–14] has received less attention, having been dismissed in a major review paper [1] on the basis of there being a large thermal expansion mismatch with the

substrate. However, the recent work by Curran and Clyne [4] has demonstrated that PEO coatings tend to have relatively low stiffness, which will limit the magnitude of thermally-induced stresses. Furthermore, the thermal conductivity of PEO coatings has been shown to be an order of magnitude lower than those of corresponding bulk crystalline oxides [14], making them potentially attractive for thermal barrier applications.

The present paper focuses on mullite-based coatings grown on aluminium alloys, using alkaline electrolytes rich in silicates. There have been some previous indications that these can be grown to greater thicknesses and at a greater rate than most other PEO coatings on aluminium, although there is little information about this in the open literature. In the present work, the structure and composition of these coatings are studied. Their stiffness and thermal expansivity are also measured. Finally their thermal conductivity is evaluated, using a steady-state method.

## 2. Experimental techniques

### 2.1. Sample preparation

Coatings were produced on a 6082 aluminium alloy, in the form of a 3 mm thick sheet, with in-plane dimensions of

\* Corresponding author.

E-mail address: [twc10@cam.ac.uk](mailto:twc10@cam.ac.uk) (T.W. Clyne).

100 mm × 50 mm, and on cylinders of a 2011 aluminium alloy 33 mm in diameter, and 20 mm in length. Coatings were prepared using a 10 kW Keronite™ processing rig and an electrolyte consisting primarily of a dilute aqueous solution of KOH and Na<sub>2</sub>SiO<sub>4</sub>. The electrolyte was maintained at a temperature of approximately 25 °C by re-circulation through a heat exchanger, with a whistle pump agitating and aerating the electrolyte. A constant capacitance condition was set, so as to achieve a current density of approximately 15 A dm<sup>-2</sup> after the initial transitory regime. Coatings were grown to a thickness of between 100 μm and 200 μm. Thicknesses were measured using an Eban 2000 eddy current thickness gauge, the accuracy of which was confirmed by occasional microscopy of cross-sections. Free-standing coatings were obtained by immersion of coated substrates in a saturated solution of NaOH for several minutes, leading to dissolution of the substrate. These samples were then rinsed in water and dried.

## 2.2. Microstructural studies

SEM observations were made using a JEOL 5800 LV and a JEOL 6340F FEGSEM. Both secondary electron (SE) and back-scattered electron (BSE) modes were used. The elemental composition of the coating was ascertained using Oxford Instruments INCA energy dispersive X-ray spectroscopy (EDS) in the JEOL 5800 SEM. A Phillips PW 1710 X-ray diffractometer was used to perform  $\theta$ – $2\theta$  scans (in Bragg–Brentano geometry) from 10° to 120°, with a 0.02 step size. A CuK $\alpha$  radiation source was used, with a 40 kV accelerating voltage and a 40 mA filament current. Data were obtained from the as-deposited free surfaces. The Hanawalt search method was used for phase identification. Phillips XPert ProFit software was then used to fit the diffraction pattern and to determine the relative integrated area under peaks corresponding to amorphous material and crystalline material. Finally, topographic studies were carried out, using a Wyko RS-2 interferometric profilometer, in order to measure the surface roughness.

## 2.3. Thermo-physical property measurement

The thermal expansion of detached coatings was investigated using a Netzsch 402L push-rod dilatometer, over the temperature range 20 to 700 °C. This allowed evaluation of the (in-plane) thermal expansivity, which was found to be approximately constant over this temperature range. Samples with a U-shaped section were used to reduce the danger of buckling, and a gauge length of ~20 mm was used.

The global in-plane Young's modulus of coatings was measured by a four-point bending of thick (~200 μm) detached coatings. Load was applied via a counter-balanced platen, using small pre-weighed masses. A brief period was allowed for the beam to settle after each addition, but both this and the timing of additions was defined, in order to standardise the effect of any small amount of creep that could have been taking place. The response to unloading was also measured, so as to ensure that the beam was still in the elastic regime.

For accurate measurement of the deflection under applied loads, a scanning laser extensometer was used, intersecting the

beam at its centre (the point of maximum deflection). This allows measurement of deflections with a resolution of about 5 μm. Together with each measurement of the nominal beam deflection (as measured up to the bottom of the beam intercept), the apparent thickness of the specimen was recorded, in order to monitor any twisting of the specimen. This could be used to correct the nominal deflection for the centreline of the specimen, but any large values suggest unevenly distributed loading and data from any such cases were discarded.

With the deflection ( $\delta$ ) measured at the centre, the bending modulus can be obtained from

$$E = \frac{Pa}{48I\delta} (3L^2 - 4a^2) \quad (1)$$

where  $L$  is the distance between the outer loading points,  $a$  is half the difference between the spans of the outer and inner loading points,  $P$  is the applied load, and  $I$  is the second moment of area of the beam section. The main factor limiting the accuracy of results obtained with this method is the precision to which specimen thickness can be measured and the effect of any non-uniformity in thickness.

## 2.4. Nanoindentation

Depth-sensitive nanoindentation was performed on polished cross-sections and in-plane sections, using a Micromaterials Nanotest 600 indenter and an MTS Nanoindenter XP. In each case, a Berkovitch indenter was used, with a maximum load of 50 mN. Hardness was calculated from load and indentation depth data, while the local stiffness was determined from the unloading response, using the standard Oliver and Pharr technique [15]. It may be noted that this stiffness differs from that measured by beam bending measurements in that: (a) it is local, and hence influenced by defects such as porosity and microcracks only if the indenter happens to probe a region containing such a defect, and (b) it is obtained under predominantly compressive loading.

## 2.5. Thermal conductivity measurements

The thermal conductivity was measured using a steady-state method. Full details are given elsewhere [16]. Three or four small (1 mm diameter) radial holes were drilled as far as the centreline in each of the two cylinders with coated ends, which were located coaxially with the coatings in contact. Thermocouples were then inserted to measure the temperature at these known points along the cylinder axis. The assembly was placed between the heating and cooling blocks of the apparatus. A small amount (~0.1 ml) of high conductivity paste was smeared at the interfaces, and a fixed torque of 2 N m was applied to the securing screw, bringing the two coated ends into good thermal contact.

Electrical resistance heating coils were then switched on (at a fixed power setting), and a steady flow of water was passed through the cooling block. Data-logging of the thermocouple output was used to determine when a steady state had been reached. Once the temperatures had been stable to within 0.5 °C for about 30 min, average thermal gradients through the

cylinders were established, allowing the temperature drop across the PEO coatings, and hence their thermal conductivity, to be determined. The thermal conductivity of the substrate materials was measured independently, and found to be  $170 \text{ W m}^{-1} \text{ K}^{-1}$  for the Al 2011. This value is known [17] to show little variation over the temperature range in question (50 to 200 °C). This allowed the heat flux through the system,  $Q$ , to be established, so that  $K$ , the effective thermal conductivity of the coating, could be obtained from

$$\frac{\Delta T}{Q} = \frac{\Delta x}{K} + \frac{1}{h} \quad (2)$$

where  $\Delta T$  is the temperature drop across the coating,  $\Delta x$  is the coating thickness, and  $h$  is the thermal conductance of the interface (including the paste).

### 3. Coating characteristics

#### 3.1. Coating structure

These coatings grow at a rate of  $\sim 0.6 \mu\text{m}/\text{min}$ , up to a thickness of  $\sim 200 \mu\text{m}$  — see Fig. 1. SEM micrographs indicated that these coatings appear to be quite dense (Fig. 2), with image analysis suggesting porosity of less than 10%. However, the recent work by Curran and Clyne [18] has demonstrated that PEO coatings tend to contain inter-connected networks of fine-scale porosity. The high resolution micrograph shown in Fig. 3 suggests that such porosity is present in the coatings being studied here.

#### 3.2. Coating composition

The application of EDX analysis in the SEM confirmed that the coatings contained Al, Si and O. This is consistent with their

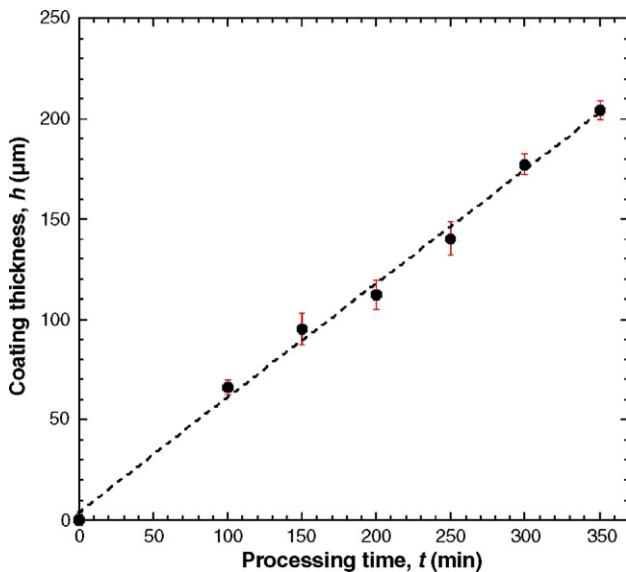


Fig. 1. Coating thickness as a function of processing time, for coatings grown using an electrolyte composition of  $10 \text{ g l}^{-1} \text{ NaSiO}_4$ ,  $10 \text{ g l}^{-1} \text{ Na}_4\text{P}_2\text{O}_7$ ,  $1.5 \text{ g l}^{-1} \text{ KOH}$ , at a current density of  $15 \text{ A dm}^{-2}$ .

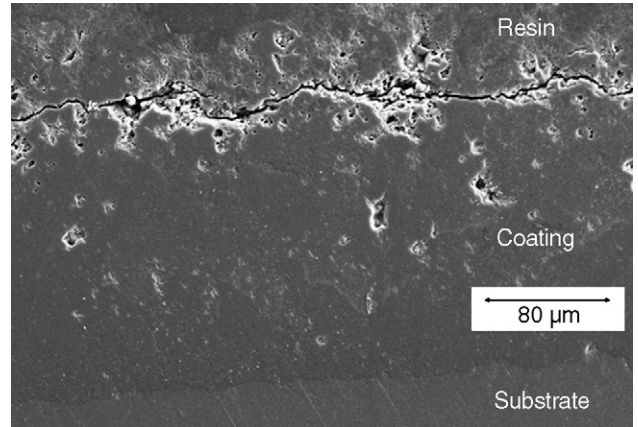


Fig. 2. SEM micrograph (SE mode) of a polished section through a  $200 \mu\text{m}$  thick PEO coating.

being composed of a mixture of mullite ( $3\text{Al}_2\text{O}_3 \cdot 2\text{SiO}_2$ ) and alumina. These composition measurements suggest approximately equal proportions of mullite and alumina. The X-ray diffraction spectrum shown in Fig. 4 confirms that mullite, and the  $\alpha$  and  $\gamma$  phases of  $\text{Al}_2\text{O}_3$ , are present, with mullite and  $\alpha$ - $\text{Al}_2\text{O}_3$  being the main crystalline constituents. Profile fitting of the low-angle amorphous peak suggests that there is approximately 30% of amorphous material in these coatings, although this could, of course, have a chemical composition including both alumina and silica.

#### 3.3. Hardness and local Young's modulus

The 50 mN indents penetrated to an approximate depth of  $2 \mu\text{m}$ . The coatings had been polished to an  $R_a$  value of about  $0.07 \mu\text{m}$ , so that the surface was smooth relative to the scale of the indents. Analysis of the indentation data indicates a hardness of  $\sim 11.5 \text{ GPa}$  and a local Young's modulus of  $\sim 170 \text{ GPa}$ . This is broadly consistent with the coatings being composed of a mixture of mullite, alumina and amorphous material.

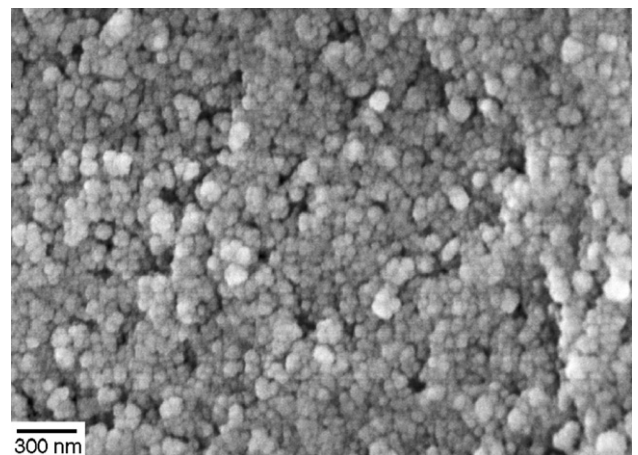


Fig. 3. SEM micrograph (SE mode, taken with a Field Emission Gun) of the free surface of a PEO coating.

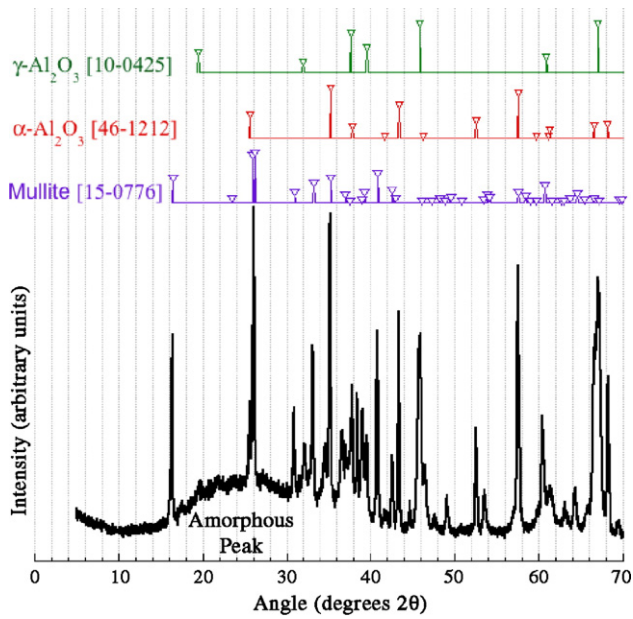


Fig. 4. X-ray diffraction spectrum (measured using Bragg–Brentano geometry), taken from a thick PEO coating, indicating the presence of amorphous material,

### 3.4. Stiffness and thermal expansion

Four-point bend testing indicated linear elastic behaviour, with a Young's modulus of  $\sim 40$  GPa, up to a strain of  $\sim 0.15$  millistrain — see Fig. 5. This is significantly less than the local modulus, just as was found for conventional alumina-based PEO coatings [4]. The low modulus is probably the result of finely-distributed pores and microcracks. This relatively high compliance will reduce the stresses induced in the coating under imposed strain, and thus promotes greater resistance to spallation during temperature changes.

The thermal expansion exhibited by the coatings was found to be linear with temperature between 200 °C and 800 °C, with an expansivity value of  $\sim 9 \times 10^{-6} \text{ K}^{-1}$ . This is higher than the expansivity of pure, crystalline mullite ( $\sim 5 \times 10^{-6} \text{ K}^{-1}$ ). The difference can be attributed to the presence of alumina and amorphous material. The expansivity mismatch between the coating and substrate ( $\alpha \approx 23 \times 10^{-6} \text{ K}^{-1}$  for aluminium) is still substantial, but, as mentioned above, the low coating modulus will reduce thermal stresses. Indeed, using the following equation

$$\frac{dU}{dA} \approx -E_c(\Delta\varepsilon)^2 t \quad (3)$$

which, using a plane strain modulus, allows the strain energy release rate (driving force for spallation) to be estimated as about  $10 \text{ J m}^{-2}$  for a 100 K temperature change, with a massive substrate and a coating thickness  $t$ , of 200  $\mu\text{m}$ . This is a relatively low driving force and, since it is clear that the fracture energy of the interface between the substrates and PEO coatings is relatively high, it follows that they are expected to be highly resistant to spallation as a result of temperature changes.

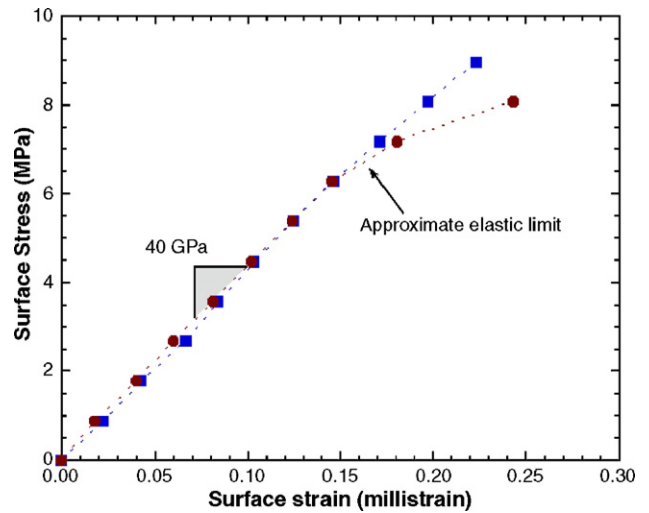


Fig. 5. Plot of surface stress against surface strain, based on the measured load-displacement data obtained during the four-point bend testing of two detached coatings.

### 3.5. Thermal conductivity

Because highly-conductive substrates like aluminium give rise to high heat fluxes, and since these coatings are relatively thin, conductivity values obtained using this experimental technique are subject to substantial error and there is considerable scatter in the data. This is illustrated by the plot of  $\Delta T/Q$  against coating thickness shown in Fig. 6. The scatter leads to relatively high uncertainty levels on the deduced values of thermal conductivity, which are  $0.25 \pm 0.09 \text{ W m}^{-1} \text{ K}^{-1}$  for unpolished coatings and  $0.52 \pm 0.17 \text{ W m}^{-1} \text{ K}^{-1}$  after polishing to remove the outer 30–40  $\mu\text{m}$  of the coating. This difference between the two sets of values is plausible, since the outer layer is known to be rather porous and friable, and would be expected to have a

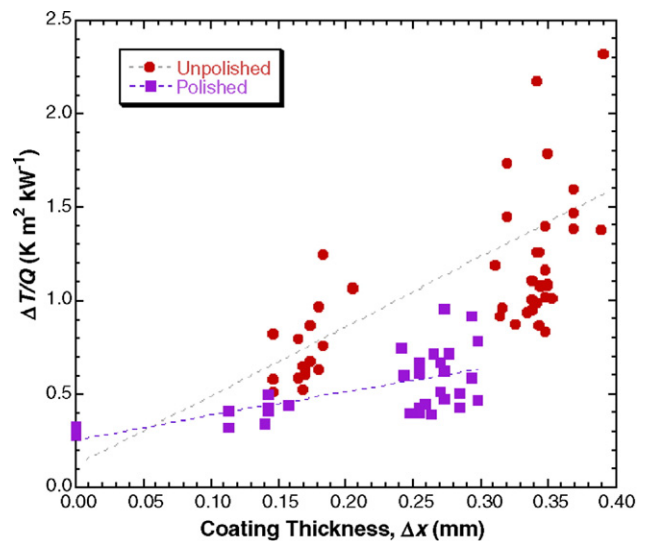


Fig. 6. Plots of  $\Delta T/Q$  against coating thickness ( $\Delta x$ ), from which the interfacial conductance,  $h$ , and the coating conductivity,  $K$ , can be deduced. Each data point represents the outcome of a single steady-state experiment. Plots are shown for both polished and unpolished coatings.

lower conductivity. However, the value for the polished coatings is probably more representative of the bulk thermal conductivity, since the lower value for the unpolished coatings may be at least partly attributable to the effect of air, contained within gaps in contact between the two blocks as a consequence of the higher surface roughness.

In any event, it may be noted that a conductivity value as low as  $0.5 \text{ W m}^{-1} \text{ K}^{-1}$  indicates that these coatings have considerable potential as thermally-insulating protective layers, particularly since they can be as thick as  $200 \mu\text{m}$  and tend to exhibit a strong resistance to spallation during thermal cycling and thermal shock. This figure is considerably below typical conductivity values for dense mullite ( $\sim 10\text{--}15 \text{ W m}^{-1} \text{ K}^{-1}$ ) and dense alumina ( $\sim 30\text{--}35 \text{ W m}^{-1} \text{ K}^{-1}$ ), but this is unsurprising in view of the very fine grain size and the presence of amorphous material and fine-scale porosity. It may be noted that a value in the range  $0.19\text{--}0.26 \text{ W m}^{-1} \text{ K}^{-1}$  has recently been reported [19] for plasma-sprayed mullite. The figure of  $0.5 \text{ W m}^{-1} \text{ K}^{-1}$  may also be compared with a recently-obtained [14] value of about  $1.6 \text{ W m}^{-1} \text{ K}^{-1}$  for alumina PEO coatings. It should also be noted that it appears to be easier to produce relatively thick PEO coatings when they are mullite-rich, since conventional alumina PEO coatings on aluminium substrates commonly have a maximum thickness of about  $100 \mu\text{m}$ . Obviously this represents an important potential advantage for mullite-rich coatings when the objective is to provide thermal protection. It's also worth noting that the PEO process is considerably cheaper, and much easier to apply to large, complex-shaped components, than the thermal spray, CVD or PVD processes.

#### 4. Conclusions

The following conclusions can be drawn from this work, relating to mullite-rich PEO coatings.

- (a) PEO coatings produced on aluminium, in an electrolyte containing KOH and sodium silicate, can readily be grown to thicknesses of  $\sim 200\text{--}250 \mu\text{m}$ . They consist primarily of mullite and alumina, plus an amorphous phase.
- (b) These coatings have a much lower thermal conductivity than the corresponding bulk crystalline materials. The measured value is about  $0.5 \text{ W m}^{-1} \text{ K}^{-1}$ , although the error on this figure may be as high as about  $0.2 \text{ W m}^{-1} \text{ K}^{-1}$ . This may be compared with the recently-obtained values for alumina PEO coatings of about  $1.6 \text{ W m}^{-1} \text{ K}^{-1}$ . These figures are approximately an order of magnitude lower than those for corresponding bulk (fully dense) materials. This is attributed to the presence of fine-scale porosity and microcracks, plus the extremely fine grain size and the presence of an amorphous phase. When considered in conjunction with the possible thickness range, it's clear that mullite-rich PEO coatings offer considerable promise as thermal barriers.
- (c) The coatings exhibit good mechanical properties, with hardness of  $\sim 10 \text{ GPa}$  and a local Young's modulus of  $\sim 170 \text{ GPa}$ . Like all PEO coatings, they adhere strongly to the substrate. They can thus be expected to exhibit good wear and impact resistance.
- (d) The global Young's modulus of the coatings is  $\sim 40 \text{ GPa}$ . This is significantly lower than that of fully dense constituent materials, and is due to the presence of microstructural defects. This low stiffness is expected to reduce the magnitude of thermally-induced stresses in the coating, increasing their resistance to spallation during thermal cycling and thermal shocking.

#### Acknowledgements

Financial support for the work described in this article has come from EPSRC and DSTL. There has also been extensive collaboration with Keronite Ltd. The authors are grateful to Dr Pavel Shashkov (Keronite), for useful discussions, and for production of some of the samples.

#### References

- [1] A.L. Yerokhin, X. Nie, A. Leyland, A. Matthews, S.J. Dowey, *Surf. Coat. Technol.* 122 (1999) 73.
- [2] X. Nie, A. Leyland, H.W. Song, A.L. Yerokhin, S.J. Dowey, A. Matthews, *Surf. Coat. Technol.* 119 (1999) 1055.
- [3] S.V. Gnedenkov, O.A. Khrisanfova, A.G. Zavidnaya, S.L. Sinebrukhov, P.S. Gordienko, S. Iwatsubo, A. Matsui, *Surf. Coat. Technol.* 145 (2001) 146.
- [4] J.A. Curran, T.W. Clyne, *Surf. Coat. Technol.* 199 (2005) 168.
- [5] A.A. Voevodin, A.L. Yerokhin, V.V. Lyubimov, M.S. Donley, J.S. Zabinski, *Surf. Coat. Technol.* 86–87 (1996) 516.
- [6] J. Tian, Z.Z. Luo, S.K. Qi, X.J. Sun, *Surf. Coat. Technol.* 154 (2002) 1.
- [7] X. Nie, E.I. Meletis, J.C. Jiang, A. Leyland, A.L. Yerokhin, A. Matthews, *Surf. Coat. Technol.* 149 (2002) 245.
- [8] L. Rama-Krishna, K.R.C. Somaraju, G. Sundararajan, *Surf. Coat. Technol.* 163–164 (2003) 484.
- [9] R. Barik, J.A. Wharton, R.J.K. Wood, K.R. Stokes, R.L. Jones, in: J. Sedriks, V. Agarwala, R. Mantz, J. Beatty (Eds.), *Tri-Service Corrosion Conference*, Navmar Applied Science Corp, Chester, PA, 2003.
- [10] T. Wei, F. Yan, J. Tian, *J. Alloys Compd.* 389 (2004) 169.
- [11] A.L. Yerokhin, X. Nie, A. Leyland, A. Matthews, *Surf. Coat. Technol.* 130 (2000) 195.
- [12] P.I. Butyagin, Y.V. Khokhryakov, A.I. Mamaev, *Mater. Lett.* 57 (2003) 1748.
- [13] S.V. Gnedenkov, O.A. Khrisanfova, A.G. Zavidnaya, S.L. Sinebrukhov, A.N. Kovryanov, T.M. Scorobogatova, P.S. Gordienko, *Surf. Coat. Technol.* 123 (2000) 24.
- [14] J.A. Curran, T.W. Clyne, *Surf. Coat. Technol.* 199 (2005) 177.
- [15] W.C. Oliver, G.M. Pharr, *J. Mater. Res.* 7 (1992) 1564.
- [16] J.C. Tan, I.O. Golosnoy, S.A. Tsipas, S. Paul, J.A. Curran, T.W. Clyne, *Use of a Steady State Bi-substrate Technique for Measurement of the Thermal Conductivity of Thick Ceramic Coatings*, *Surf. Coat. Technol.* (in press).
- [17] F.P. Incropera, D.P. Dewitz, *Fundamentals of Heat and Mass Transfer*, John Wiley & Sons, 2002.
- [18] J.A. Curran, T.W. Clyne, *Acta Mater.* 54 (2006) 1985.
- [19] S. Seifert, E. Litovsky, J.I. Kleiman, R.B. Heimann, *Surf. Coat. Technol.* 200 (2006) 3404.